NASA TECHNICAL NOTE

NASA TN D-5363

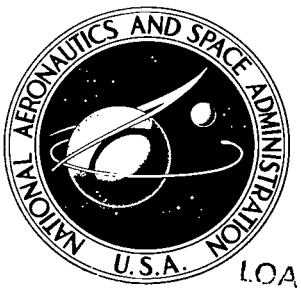

NASA TN D-5363

AN ANALYTICAL EVALUATION OF THE DENTING OF AIRPLANE SURFACES BY HAIL

by Robert G. Thomson and Robert J. Hayduk

Langley Research Center
Langley Station, Hampton, Va.

NATIONAL AERONAUTICS AND SPACE ADMINISTRATION • WASHINGTON, D. C. • AUGUST 1969

1. Report No. NASA TN D-5363	2. Government Accession No.	3. Recipient's Catalog No.
4. Title and Subtitle AN ANALYTICAL EVALUATION OF THE DENTING OF AIRPLANE SURFACES BY HAIL		5. Report Date August 1969 6. Performing Organization Code
7. Author(s) Robert G. Thomson and Robert J. Hayduk		8. Performing Organization Report No. L-6494
9. Performing Organization Name and Address NASA Langley Research Center Langley Station Hampton, Va. 23365		10. Work Unit No. 126-61-01-07-23 11. Contract or Grant No.
12. Sponsoring Agency Name and Address National Aeronautics and Space Administration Washington, D.C. 20546		13. Type of Report and Period Covered Technical Note 14. Sponsoring Agency Code
15. Supplementary Notes		

16. Abstract

Hailstone damage to aircraft is exhibited as denting or complete penetration. An analytical evaluation of such denting characteristics of aircraft surfaces is idealized by having a crushable spherical projectile impact normal to a flat plate. Separate elastic and rigid-plastic analyses have been developed previously by using the classical thin-plate bending approach. As applied in this paper, the elastic analysis determines the area of the sheet around the center of impact, which has become plastic. The rigid-plastic analysis applied to this central plastic region determines the resulting permanent deformation (dent). Numerical results are presented in detail for the permanent deformations of two specific sheet thicknesses.

17. Key Words Suggested by Author(s) Impulse loading Plastic deformations Elastic deformations Thin sheets Dynamic Hailstone dents	18. Distribution Statement Unclassified – Unlimited

19. Security Classif. (of this report) Unclassified	20. Security Classif. (of this page) Unclassified	21. No. of Pages 34	22. Price* $3.00

*For sale by the Clearinghouse for Federal Scientific and Technical Information Springfield, Virginia 22151

AN ANALYTICAL EVALUATION OF THE DENTING OF AIRPLANE SURFACES BY HAIL

By Robert G. Thomson and Robert J. Hayduk
Langley Research Center

SUMMARY

Hailstone damage to airplanes is exhibited as denting or complete penetration. An analytical evaluation of such denting characteristics of airplane surfaces is idealized by having a crushable spherical projectile impact normal to a flat plate. Separate elastic and rigid-plastic analyses have been developed previously by using the classical thin-plate bending approach. As applied in this paper, the elastic analysis determines the area of the sheet around the center of impact, which has become plastic. The rigid-plastic analysis applied to this central plastic region determines the resulting permanent deformation (dent). Numerical results are presented in detail for the permanent deformations of two specific sheet thicknesses.

INTRODUCTION

Because of the high velocity of modern airplanes, the probability of surface damage caused by impact with hail, and possibly with other meteorological precipitants, has become a design consideration. Meteorological damage can take the form of either surface-material erosion, permanent deformation, or, if the impact is severe enough, complete penetration of the surface. A summary of the effect of hail on airplanes in flight with photographic documentation of damage and an extensive bibliography is given in reference 1.

No design criterion for hail encounter has been available to the aircraft designers until recently. In reference 2 a testing procedure is proposed to aid the designer in minimizing hail damage. The suggested approach is to test the affected structure by impacting it with representative samples of hail at various impact velocities to assure that no appreciable damage occurs. An analytical approach does not appear to be available, and the purpose of the present paper is to present an approximate analytical method to complement established laboratory testing procedures.

When a hailstone impacts the thin skin of an airplane, the resulting skin deformations usually are plastic near the point of impact and elastic in the surrounding area. If

the impact is severe enough, both bending and membrane action are present in the skin. A rigorous, but difficult, approach to the problem would require a sophisticated, dynamic, elastic-plastic, large-deformation analysis. The analytical development in this paper, however, attempts to approximate the analysis of the problem to circumvent the difficulties of the more rigorous approach.

In reference 3 an elastic analysis was developed by using the classical thin-plate bending approach for the impact of a spherical projectile on a thin infinite sheet. The results of that analysis determine the time-dependent expressions for the deformation, velocity, and moment distributions of the elastically deforming sheet. The elasticity assumptions, however, preclude any permanent-type deformations.

The rigid-plastic bending response of a finite circular sheet subjected to a transverse impulse loading has also been investigated. (See ref. 4.) The rigid-plastic analysis considers the entire finite sheet as plastic, and when deformations occur, the whole sheet experiences a permanent type of deformation. Therefore, in regard to hailstone impact, if the extent of the plastic area around the center of impact is known, a rigid-plastic analysis can be used to predict the permanent-deformation characteristics (denting) of this region.

In the present paper the elastic analysis of reference 3 is used to determine the radial and circumferential bending-moment distributions in an infinite elastic sheet impacted by a crushable spherical projectile. A rigid-plastic analysis is also developed herein for a simply supported finite circular sheet impacted by a crushable spherical projectile, and the resulting permanent deformation is found. The two analyses have identical initial conditions on loading: a crushable spherical projectile in which the projectile is assumed to impose an initial, instantaneous, finite velocity distribution over the region of impact, the rest of the plate being at rest. In both analyses the circumferential and radial moments are at a maximum at the center of the impact and decrease monotonically with increasing radius. For the infinite elastic sheet the bending moments around the center of impact are shown to exceed the dynamic elastic yield-moment resultant M_O.

In the present approach the simply supported, rigid-plastic boundary conditions on the radial and circumferential bending moments of the plastic analysis are matched with those of the elastic analysis at some radius near the center of impact called the plastic radius. The rigid-plastic analysis, using this plastic radius as the radius of the finite circular sheet, is then to be used to determine the permanent deformations. The principal contention of the present paper is that sufficiently accurate results may be obtained when only the boundary conditions on the bending moments are satisfied between the elastic and plastic analyses in determining the plastic radius.

The permanent deformations on the rigid-plastic sheet increase with increasing hailstone size and velocity. However, it is recognized that a failure by perforation occurs at a certain critical impact velocity and that this failure results in a practical limit to the deformations. This practical limit can be established once experimental data become available on the dynamic material properties associated with hailstone impact. A preliminary estimate of the location of this limit is presented in this paper.

SYMBOLS

The units used for the physical quantities defined in this paper are given both in U.S. Customary Units and in the International System of Units (SI). (See ref. 5.) Appendix A presents factors relating these two systems of units.

a radius of projectile

b radius of central plastic region

$c = \sqrt{E/\rho_t}$

D flexural rigidity of sheet, $Eh^3/12(1 - \nu^2)$

E elastic modulus of sheet material in tension and compression

g_o projectile velocity

h target thickness

$J_n(z)$ Bessel function of the first kind

$k = \frac{2a^2}{ch}\sqrt{3(1 - \nu^2)}$

$\dot{k}_r, \dot{k}_\theta$ radial and circumferential time rates of curvature

M bending-moment resultant

M_o yield-moment resultant, $\sigma_o(h/2)^2$; maximum bending moment that sheet can sustain

m mass

p Hankel transform parameter

Q_r transverse shear-stress resultant

q impulse loading

r,θ,z radial, circumferential, and transverse coordinates, respectively (see fig. 1)

t time

t^* time of cessation of all sheet motion after impact

t_1 time at which hinge-circle radius has decreased to zero

$$V_o = \frac{\frac{2a}{h}\frac{\rho_p}{\rho_t} g_o}{1 + \frac{2a}{h}\frac{\rho_p}{\rho_t}\psi}$$

w sheet deflection in transverse direction (z-direction)

δ permanent center deflection, $w(0,t^*)$

ζ radius of hinge circle separating regimes A and AB

$\eta = r/a$

μ mass per unit area of sheet, $\rho_t h$

ν Poisson's ratio

$\xi = r/b$

ρ mass density

σ_o yield stress in simple tension or compression (assumed to be identical in magnitude)

σ_r,σ_θ principal radial and circumferential stresses, respectively

$\tau = t/k$

ψ momentum constant (see eq. (7))

Subscripts:

cr critical

n indicates order of Bessel function

p projectile

r radial

t target

θ circumferential

A dot over a symbol indicates partial differentiation with respect to time t. An asterisk denotes time at which the entire sheet comes to rest.

MATHEMATICAL ANALYSES

Determination of Initial Velocity Distribution

Linear, small-deflection plate theory was used in reference 3 to study the response of an infinite elastic sheet subjected to an axisymmetric impulse. The analysis assumed that the momentum exchange was the primary loading mechanism, that the exchange was instantaneous, and that the mass of the projectile was negligible after impact compared with the mass of the sheet. The three specific projectile shapes studied in reference 3 were cone, sphere, and cylinder. Reference will be made in this paper to the solution for the spherical projectile only, and the momentum distribution shown in figure 1 is derived from this shape.

The assumed instantaneous momentum exchange between projectile and sheet yields an initial sheet velocity over the centrally impacted area, but no initial displacement. In the present analysis the mass of the projectile after impact is not neglected as in reference 3. The momentum balance for a completely inelastic impact is

$$\left(m_p + m_t\right)\dot{w}(\eta,0) = m_p g_o \tag{1}$$

or, from figure 1

$$\left[2\pi a^2\eta\left(2a\sqrt{1-\eta^2}\right)\rho_p\,d\eta + 2\pi a^2\eta h\rho_t\,d\eta\right]\dot{w}(\eta,0) = 2\pi a^2\eta\left(2a\sqrt{1-\eta^2}\right)\rho_p\,d\eta\,g_o \tag{2}$$

Solution of equation (2) for the initial velocity distribution $\dot{w}(\eta,0)$ gives

$$\left.\begin{aligned} \dot{w}(\eta,0) &= \frac{\frac{2a}{h}\frac{\rho_p}{\rho_t}g_o\sqrt{1-\eta^2}}{1+\frac{2a}{h}\frac{\rho_p}{\rho_t}\sqrt{1-\eta^2}} && (0 \leqq \eta \leqq 1) \\ \dot{w}(\eta,0) &= 0 && (\eta \geqq 1) \end{aligned}\right\} \tag{3}$$

An approximation to this initial velocity distribution is made to utilize the results of reference 3 in which the initial velocity is assumed to be of the form:

$$\left.\begin{aligned} \dot{w}(\eta,0) &= \left(\frac{2a}{h}\frac{\rho_p}{\rho_t}g_o\right)\sqrt{1-\eta^2} && (0 \leqq \eta \leqq 1) \\ \dot{w}(\eta,0) &= 0 && (\eta \geqq 1) \end{aligned}\right\} \tag{4}$$

In this approximation the character of equation (4) is retained but the mass of the projectile after impact is included. The approximation to equation (3) is

$$\left.\begin{aligned} \dot{w}(\eta,0) &= V_o\sqrt{1-\eta^2} && (0 \leqq \eta \leqq 1) \\ \dot{w}(\eta,0) &= 0 && (\eta \geqq 1 \end{aligned}\right\} \tag{5}$$

where

$$V_o = \frac{\frac{2a}{h}\frac{\rho_p}{\rho_t}g_o}{1+\frac{2a}{h}\frac{\rho_p}{\rho_t}\psi}$$

The momentum constant ψ is determined by equating the total momentum of the sheet for two sheet initial velocity distributions. In one case, the exact velocity distribution (eq. (3)) is employed in the momentum equation. In the other case, the approximate velocity distribution (eq. (5)) is used; that is,

$$\int_0^1 \frac{\sqrt{1-\eta^2}}{1+\frac{2a}{h}\frac{\rho_p}{\rho_t}\sqrt{1-\eta^2}}\eta\,d\eta = \int_0^1 \frac{\sqrt{1-\eta^2}}{1+\frac{2a}{h}\frac{\rho_p}{\rho_t}\psi}\eta\,d\eta \tag{6}$$

and the momentum constant ψ becomes

$$\psi = \frac{1}{\frac{3}{2} - \frac{3}{\frac{2a}{h}\frac{\rho_p}{\rho_t}} + \frac{3}{\left(\frac{2a}{h}\frac{\rho_p}{\rho_t}\right)^2}\ln\left(1+\frac{2a}{h}\frac{\rho_p}{\rho_t}\right)} - \frac{1}{\frac{2a}{h}\frac{\rho_p}{\rho_t}} \tag{7}$$

The values of ψ used in the specific calculations in this paper are presented in table I along with the target (2024-T4 aluminum) and projectile material (ice) properties. A comparison of the exact initial velocity distribution (eq. (3)) with the approximate initial velocity distribution (eq. (5)) is shown in figure 2 for a 0.25-inch-radius (0.64-cm) hailstone impacting a 0.063-inch-thick (0.160-cm) plate ($\psi = 0.71$).

Determination of Moments in the Elastic Region

The boundary conditions of zero deflection, slope, and shear per unit length at infinity and of zero slope and finite shear at the origin were assumed in reference 3 in order to obtain a solution in single integral form for the deflection of the dynamically deforming plate. The deflection (eq. (31) of ref. 3) can be written as

$$w = k\frac{2a}{h}\left(\frac{\rho_p}{\rho_t}g_o\right)\sqrt{\frac{\pi}{2}}\int_0^\infty p^{-5/2}J_{3/2}(p)\,J_0(p\eta)\,\sin\left(p^2\tau\right)dp \tag{8}$$

where in the present paper $\frac{2a}{h}\frac{\rho_p}{\rho_t}g_o$ will be replaced by V_o. The expressions for the radial and circumferential moments from elasticity theory are, respectively,

$$M_r(\eta,\tau) = -\frac{D}{a^2}\left(\frac{\partial^2 w}{\partial\eta^2} + \frac{\nu}{\eta}\frac{\partial w}{\partial\eta}\right) \tag{9}$$

$$M_\theta(\eta,\tau) = -\frac{D}{a^2}\left(\frac{1}{\eta}\frac{\partial w}{\partial\eta} + \nu\frac{\partial^2 w}{\partial\eta^2}\right) \tag{10}$$

The radial and circumferential moments for $\nu = 1/3$ (eqs. (8), (9), and (10) combined) can be written in the form (see appendix B):

$$M_r(\eta,\tau) = -\frac{DkV_o\sqrt{\frac{\pi}{2}}}{6a^2}\int_0^\infty J_{3/2}(p)\,\sin\left(p^2\tau\right)p^{-1/2}\left\{3\left[J_2(p\eta) - J_0(p\eta)\right] - \frac{2}{\eta}p^{-1}\,J_1(p\eta)\right\}dp \qquad (11)$$

$$M_\theta(\eta,\tau) = -\frac{DkV_o\sqrt{\frac{\pi}{2}}}{6a^2}\int_0^\infty J_{3/2}(p)\,\sin\left(p^2\tau\right)p^{-1/2}\left[-\frac{6}{\eta}p^{-1}\,J_1(p\eta) + J_2(p\eta) - J_0(p\eta)\right]dp \qquad (12)$$

and, for $\eta = 0$, they reduce to

$$M(0,\tau) = \frac{2DkV_o\sqrt{\frac{\pi}{2}}}{3a^2}\int_0^\infty J_{3/2}(p)\,\sin\left(p^2\tau\right)p^{-1/2}\,dp \qquad (13)$$

The nondimensional radial and circumferential moment distributions $\frac{M_r(\eta,\tau)}{M(0,\tau)}$ and $\frac{M_\theta(\eta,\tau)}{M(0,\tau)}$, respectively, in the central portion of the infinite elastic sheet (center of impact) are plotted in figure 3.

Rigid-Plastic Analysis

In reference 4 the dynamic rigid-plastic response of a thin, circular plate to an axisymmetric impulse loading with radial variation was considered. Specifically, the radial impulse loading had a Gaussian distribution. The circular sheet was assumed to be finite in extent, simply supported along its outer edge, and uniform in thickness. The sheet was also assumed to be composed of a material that is incompressible, ideally plastic (no work-hardening), and isotropic in yielding. Only the bending action of the plate was considered; the elastic deformations as well as the membrane forces were neglected. The rigid, perfectly plastic plate material was assumed to deform according to the Tresca yield condition and the associated flow rule. (See ref. 4.)

The present analysis is similar to the analysis of reference 4. However, the axisymmetric loading function is no longer Gaussian but is replaced by a projected spherical impulse distribution, and the effect of the mass of the projectile is not neglected after impact but is accounted for approximately as in the previously discussed elastic analysis. Hence, the rigid-plastic plate, which is initially at rest, immediately upon impact assumes a velocity distribution as given by equation (5); and both the elastic and rigid-plastic plate analyses have identical initial conditions:

$$w(\eta,0) = 0$$

$$\dot{w}(\eta,0) = V_o\sqrt{1 - \eta^2} \qquad (0 \leqq \eta \leqq 1)$$

$$\dot{w}(\eta,0) = 0 \qquad (\eta \geqq 1)$$

The details of the rigid-plastic solution are given in appendix C. The permanent deformation of the rigid-plastic plate can be written as

$$w^*(\xi,t^*) = \frac{\mu V_o{}^2 b^2}{24M_o}\left\{\left[1 - \left(\frac{\xi}{a/b}\right)^2\right]^{1/2} \frac{24M_o}{\mu V_o b^2} t(\xi) + (1 - \xi)\left[1 + 2\xi + 3\xi^2 - \left(\frac{b}{a}\right)^2 \xi^2 - 2\left(\frac{b}{a}\right)^2 \xi^3\right]\right\}$$

$$\left(0 \leqq \xi \leqq \frac{\zeta(0)}{b}\right) \qquad (14)$$

$$w^*(\xi,t^*) = \frac{\mu V_o{}^2 b^2}{24M_o}(1 - \xi)\left[1 + \left(\frac{a}{b}\right)^2 + \left(\frac{a}{b}\right)^4\right] \qquad \left(\frac{\zeta(0)}{b} \leqq \xi \leqq 1\right) \qquad (15)$$

where the permanent center deformation δ is expressed as (see fig. 1)

$$\delta = w^*(0,t^*) = \frac{\mu V_o{}^2 b^2}{24M_o}\left(1 + \frac{24M_o}{\mu V_o b^2} t_1\right) \qquad (16)$$

and $\xi = r/b$, b is the radius of the plastic plate, and a is the radius of the projectile. The nondimensional time parameter $\frac{24M_o}{\mu V_o b^2} t_1$ (see eq. (C9)) for $0 \leqq a/b \leqq 1$ is

$$\frac{24M_o}{\mu V_o b^2} t_1 = -2 + 8\left(\frac{a}{b}\right)^2 + \sqrt{1 - \left(\frac{a}{b}\right)^2}\left[2 - 6\left(\frac{a}{b}\right)^2 + \left(\frac{a}{b}\right)^4\right] - 3\left(\frac{a}{b}\right)^3 \sin^{-1}\left(\frac{a}{b}\right) \qquad (17)$$

and for $a/b \geqq 1$ (that is, projectile larger than plastic dent) is (see eq. (C10))

$$\frac{24M_o}{\mu V_o b^2} t_1 = -2 + 8\left(\frac{a}{b}\right)^2 + \sqrt{1 - \left(\frac{b}{a}\right)^2}\left[2 - 5\left(\frac{a}{b}\right)^2\right] - 3\left(\frac{a}{b}\right)^3 \sin^{-1}\left(\frac{b}{a}\right) \qquad (18)$$

Also, the nondimensional time parameter $\frac{24M_o}{\mu V_o b^2} t(\xi)$ is expressed as (see eq. (C11)):

$$\frac{24M_o}{\mu V_o b^2} t(\xi) = \left[1 - \left(\frac{\xi}{a/b}\right)^2\right]^{1/2}\left[-2 + 8\left(\frac{a}{b}\right)^2 - 2\xi + 2\xi^2 - 3\left(\frac{a}{b}\right)^2 \xi\right]$$

$$+ 3\left(\frac{a}{b}\right)^3 \sin^{-1}\left(\frac{\xi}{a/b}\right) + 2 - 8\left(\frac{a}{b}\right)^2 + \frac{24M_o}{\mu V_o b^2} t_1 \qquad (19)$$

RESULTS AND DISCUSSION

Determination of Radius of Plastic Center

The simple-support boundary conditions of the rigid-plastic sheet, according to plasticity theory (see appendix C), are that the radial moment M_r equal zero and the circumferential moment M_θ equal M_o. Hence, the particular radial location b/a of the central plastic portion of the infinite elastic sheet was taken to be at the radial location where $M_r = 0$; this radial location changes with time. For different specific times the value of the circumferential moment M_θ at the radial location where $M_r = 0$ will possess values that range from above to below the yield moment M_o (assuming that the sheet and hailstone properties remain constant). When $M_\theta = M_o$ (with $M_r = 0$), and only then, are the boundary conditions met for the simply supported plastic sheet; and it follows that this radius is the only radius of plastic yielding on the elastic sheet at which the boundary conditions are satisfied.

Typical ($\tau = 1.5$) radial (eq. (11)) and circumferential (eq. (12)) moment distributions in the central portion of the infinite elastic sheet are plotted in figure 3. The maximum (and only) radius of the rigid-plastic region for a particular hailstone-sheet combination is determined inversely by matching the rigid-plastic boundary conditions at a particular radius of the infinite elastic sheet. For example, in figure 3 b/a is chosen to be at the radial location $\eta = 2.74$ where $M_r = 0$; the value of M_θ at $\eta = 2.74$ depends on the sheet and hailstone properties. If the sheet and hailstone properties are then selected so that M_θ equals M_o, the yield moment, then the radius of the rigid-plastic sheet b/a equals 2.74 for this particular hailstone-sheet combination. Hence, any elastic moment distribution specifies the radius of a rigid-plastic sheet for a particular hailstone diameter, plate thickness, and material when the hailstone velocity is selected to make the elastic circumferential moment M_θ (eq. (12)) equal to the yield moment M_o.

By calculating various moment distributions at a number of specific times, such as the one shown in figure 3, and applying the criterion for determining the maximum radius of plastic yielding (shown as the dashed line in fig. 3), a relationship between b/a and the initial projectile velocity can be established. Such a relationship is shown plotted in figure 4 for three different hailstones of 0.50-, 0.25-, and 0.125-inch radius (1.27-, 0.64-, and 0.32-cm). In figure 4 two typical aircraft skin thicknesses were chosen as target-plate thicknesses: 0.04 inch (0.10 cm), shown as the solid line, and 0.063 inch (0.160 cm), shown as the dashed line, respectively. The nondimensional plastic radius is shown in figure 4 to increase, for a particular velocity, as either the target thickness decreases and/or the projectile radius increases. Also, the plastic radius increases as the projectile velocity increases, as is expected.

At extremely small values of τ (that is, $\tau \leqq 0.2$) corresponding to values of $b/a > 1$, it should be noted, however, that an anomaly occurs in the moment distributions. Since it is known that classical plate theory predicts a spurious response at all points of a plate immediately after the application of a sharp impulse (ref. 6), the anomaly in the moment distributions is felt to be mathematical rather than physical. The anomaly tends to distort the smooth monotonically decreasing form of the moment distributions as presented in figure 3 and also the computed values of the plastic radius as shown in figure 4. The computed values of the plastic radius begin to oscillate as b/a decreases below 0.5, and the curves presented in figure 4 have been faired between $b/a = 0.5$ and $b/a = 0$. The value of the projectile velocity at $b/a = 0$ can be easily (and accurately) determined by setting $M(0,\tau)$ in equation (13) equal to M_0. Fortunately, this oscillation in the computed values of b/a occurs in the region where the plastic dent has a smaller radius than the impacting hailstone and generally is of less interest than in the region where $b/a > 1$.

Determination of Permanent Center Deformation

The radius b, which is the maximum radius of plastic yielding from the elastic analysis, is now to be used as the finite radius of the rigid-plastic plate. By use of equation (16) and the appropriate values of a, b, h, M_0, μ, and others (see table I) for target and projectile material properties, the permanent center deflection δ of the plastically deformed plate is determined. In figure 5, a logarithmic plot of the permanent center deformation as a function of projectile velocity is shown for three different hailstones of 0.50-, 0.25-, and 0.125-inch radius (1.27-, 0.64-, and 0.32-cm) and with a target-sheet thickness of 0.063 inch (0.160 cm). The permanent center deformation is seen to approach a linear asymptote (shown as a dashed line) as the projectile velocity increases for the three sizes of hailstones. This linear asymptote has a constant slope of 2.85. The permanent center deformation is also shown to be very sensitive to projectile size, probably because of the thinness of the target sheet relative to the mass of the hailstones.

In figure 6 the shape of the permanent deformation is plotted (eqs. (14) and (15)) for three specific projectile impact velocities of the 0.50-inch-radius (1.27-cm) hailstone. The projectile velocities are 330, 500, and 1100 ft/sec (0.10, 0.15, and 0.34 km/s) and show a progression from a shallow, circular, dish-shaped dent to a deep conical cavity. Thus, the shape of the dent, as well as the center deformation, changes as the projectile velocity is varied. The limited damage information available (ref. 1) indicates that the indentation predictions of the analysis are reasonable; however, adequate data for comparison are not available.

In figure 7, a logarithmic plot of the permanent center deformation as a function of projectile velocity is shown for hailstones of 0.50-, 0.25-, and 0.125-inch radius (1.27-, 0.64-, and 0.32-cm) but for a target-sheet thickness of 0.04 inch (0.10 cm). The permanent center deformation is again seen to approach a linear asymptote as the projectile velocity increases, in fact, the same asymptote as in figure 5. From the results given in figures 5 and 7 it is apparent that the permanent center deformation, in the high velocity range, is a function of the projectile velocity g_o raised to the 2.85 power. In an attempt to show the six curves given in figures 5 and 7 on a single curve, the permanent center deformation is plotted as a function of $g_o a/h^{2/3}$ in figure 8 to a logarithmic scale. The curves in figure 8 show a general tendency toward a common linear asymptote in the high velocity range, but some spread does exist among the curves. This spread can be attributed, in part, to the choice of the abscissa parameter $g_o a/h^{2/3}$.

Critical Impact Velocity

The critical impact velocity is defined as the minimum impact velocity for a given sheet and projectile combination that barely allows the projectile to perforate the sheet. An analytical expression for the critical impact velocity of a thin sheet impacted by a spherical projectile is presented in reference 7. It was derived from the elastic response of the sheet by assuming a failure criterion based on a maximum fracture stress. The critical impact velocity of a thin visco-plastic sheet impacted by a cylindrical projectile was studied in reference 8. By comparing the results presented in references 7 to 10, it can be shown that the relation between the critical sheet thickness and the critical impact velocity is linear, as is reported in both the elastic and visco-plastic analyses. The following analytical relationship (ref. 7) is felt to be a reasonable statement of proportionality to determine the critical sheet thickness h_{cr} for thin sheets impacted by spherical projectiles:

$$h_{cr} \propto \frac{m(g_o)_{cr}}{a^2\sqrt{\rho_t}} \tag{20}$$

A proportionality constant, which would be a function of the sheet material properties, can be determined once meaningful experimental data on the dynamic material properties of thin sheets impacted with hailstones become available. Limiting ballistic envelopes are plotted in figures 5 and 7 as the long-short, dashed curves. The shape of this limiting envelope is presumed to be known at present; its location has been estimated and is subject to change.

CONCLUDING REMARKS

The present analysis, although not an exact elastic-plastic treatment, has combined separate elastic and rigid-plastic analyses to study hail damage to airplane surfaces. The results of this analysis indicate that thin structural members, such as the large skin areas of airplanes are quite susceptible to denting by hailstones. The larger the hailstone the greater the damage, of course, but the analysis also indicates great sensitivity to impact velocity as the hailstone size increases. In fact, the permanent center of deformation of an impacted skin has been shown to approach a function of the impact velocity to the 2.85 power for center deformations of 0.10 inch (0.25 cm) or over.

The analytical results presented herein must await experimental verification. Although the magnitudes of the permanent deformations may be found to be in need of adjustment because of the neglect of membrane action and the numerous simplifying assumptions of the present analysis, it is hoped that the parametric study made herein and especially the impact-velocity dependency uncovered may prove to be useful. It is realized also that the results presented are for normal impact onto flat sheets, and that some of the most severe hail damage to aircraft occurs at the leading edge of wing and tail assemblies, which are highly curved. The strengthening and geometric factors connected with curvature of the sheet need to be evaluated. It is suggested that for oblique impact the normal component of the impact be considered as a first approximation.

Perforation of the airplane skin occurs at some critical impact velocity, but the prediction by analysis of the magnitude of this impact velocity awaits experimental determination of some material properties at impact conditions.

Langley Research Center,
National Aeronautics and Space Administration,
Langley Station, Hampton, Va., May 15, 1969,
126-61-01-07-23.

APPENDIX A

CONVERSION OF U.S. CUSTOMARY UNITS TO SI UNITS

The International System of Units (SI) was adopted by the Eleventh General Conference on Weights and Measures, Paris, October 1960, in Resolution No. 12 (ref. 5). Conversion factors for the units used herein are given in the following table:

Physical quantity	U.S. customary unit	Conversion factor (a)	SI unit
Length	in.	0.0254	meters (m)
Density	lbm/ft^3	16.02	kilograms per cubic meter (kg/m^3)
Stress	psi (lbf/in^2)	6.895×10^3	newtons per square meter (N/m^2)
Velocity	ft/sec	0.3048	meters per second (m/s)

[a]Multiply value given in U.S. customary unit by conversion factor to obtain equivalent value in SI unit.

Prefixes to indicate multiple of units are as follows:

Prefix	Multiple
centi (c)	10^{-2}
kilo (k)	10^3
giga (G)	10^9

APPENDIX B

MOMENT EXPRESSIONS FOR CRUSHABLE SPHERICAL PROJECTILE

The expressions for the radial and circumferential moments of an elastic plate from elasticity theory are, respectively (see eqs. (9) and (10)),

$$M_r(\eta,\tau) = -\frac{D}{a^2}\left(\frac{\partial^2 w}{\partial \eta^2} + \frac{\nu}{\eta}\frac{\partial w}{\partial \eta}\right) \tag{B1}$$

$$M_\theta(\eta,\tau) = -\frac{D}{a^2}\left(\frac{1}{\eta}\frac{\partial w}{\partial \eta} + \nu\frac{\partial^2 w}{\partial \eta^2}\right) \tag{B2}$$

The elastic deflection in single-integral form is (eq. (8))

$$w = kV_o\sqrt{\frac{\pi}{2}}\int_0^\infty p^{-5/2}\, J_{3/2}(p)\, J_0(p\eta)\, \sin\left(p^2\tau\right) dp \tag{B3}$$

Hence, the radial and circumferential moments (by substitution of eq. (B3) into eqs. (B1) and (B2)) become

$$M_r(\eta,\tau) = -\frac{DkV_o\sqrt{\frac{\pi}{2}}}{a^2}\int_0^\infty J_{3/2}(p)\, \sin\left(p^2\tau\right)\left\{\frac{1}{2}p^{-1/2}\left[J_2(p\eta) - J_0(p\eta)\right] - \frac{\nu}{\eta}p^{-3/2}\, J_1(p\eta)\right\} dp \tag{B4}$$

$$M_\theta(\eta,\tau) = -\frac{DkV_o\sqrt{\frac{\pi}{2}}}{a^2}\int_0^\infty J_{3/2}(p)\, \sin\left(p^2\tau\right)\left\{-\frac{p^{-3/2}}{\eta}J_1(p\eta) + \frac{\nu}{2}p^{-1/2}\left[J_2(p\eta) - J_0(p\eta)\right]\right\} dp \tag{B5}$$

The evaluation of M_r and M_θ at $\eta = 0$ is determined by noting that

$$\lim_{\eta \to 0}\frac{dJ_1(p\eta)}{d\eta} = \left[\frac{J_0(p\eta) - J_2(p\eta)}{2}\right]p\Bigg|_{\eta \to 0} = \frac{p}{2} \tag{B6}$$

$$\lim_{\eta \to 0}\frac{J_1(p\eta)}{\eta} = \left[\frac{J_2(p\eta) + J_0(p\eta)}{2}\right]p\Bigg|_{\eta \to 0} = \frac{p}{2} \tag{B7}$$

APPENDIX B

If ν is taken to be equal to 1/3, equations (B4) and (B5) reduce to

$$M_r(0,\tau) = M_\theta(0,\tau) = M(0,\tau) = \frac{2}{3}\frac{DkV_o}{a^2}\sqrt{\frac{\pi}{2}}\int_0^\infty J_{3/2}(p)\,\sin\left(p^2\tau\right)\,p^{-1/2}\,dp \tag{B8}$$

The nondimensional radial and circumferential moments, respectively, can then be written as

$$\frac{M_r(\eta,\tau)}{M(0,\tau)} = \frac{-\frac{1}{4}\int_0^\infty J_{3/2}(p)\,\sin\left(p^2\tau\right)\,p^{-1/2}\left\{3\left[J_2(p\eta) - J_0(p\eta)\right] - \frac{2}{\eta}p^{-1}\,J_1(p\eta)\right\}dp}{\int_0^\infty J_{3/2}(p)\,\sin\left(p^2\tau\right)\,p^{-1/2}\,dp} \tag{B9}$$

$$\frac{M_\theta(\eta,\tau)}{M(0,\tau)} = \frac{-\frac{1}{4}\int_0^\infty J_{3/2}(p)\,\sin\left(p^2\tau\right)\,p^{-1/2}\left\{-\frac{6}{\eta}p^{-1}\,J_1(p\eta) + \left[J_2(p\eta) - J_0(p\eta)\right]\right\}dp}{\int_0^\infty J_{3/2}(p)\,\sin\left(p^2\tau\right)\,p^{-1/2}\,dp} \tag{B10}$$

APPENDIX C

RIGID-PLASTIC SOLUTION FOR SPHERICAL PROJECTILE IMPACT

The analytical derivation of the deflection of the plastically deforming, simply supported circular plate presented in this appendix is similar in approach to existing dynamic rigid-plastic solutions. The development of the governing equations closely parallels that of reference 4, except for a change in the functional form of the initial velocity distribution across the plate. (For a more complete discussion of rigid-plastic theory of plasticity, utilizing the Tresca yield condition and the associated flow rule, the reader is referred to reference 4.) The development of the deflection expressions for the plastically deforming plate is divided in this appendix into two sections. The first section presents the solution for the motion of the plate when the plate is divided into two distinct plasticity regimes, separated by a hinge circle, up to the time of the disappearance of this hinge circle. The second section contains the solution for the motion of the plate as it continues to deform, up to the time of cessation of all motion. Both sections will be as brief and concise as possible because the analytical development is similar to that presented in reference 4, and a more complete treatment is not deemed to be necessary.

Solution With Hinge Circle of Finite Radius

The rigid-plastic plate, which is initially at rest, immediately upon impact assumes an axisymmetric velocity distribution in the central portion of the plastic plate (designated regime A of the Tresca yield hexagon in fig. 9) of the form

$$\dot{w}(\eta,0) = V_0\sqrt{1 - \left(\frac{b}{a}\right)^2\xi^2} \qquad \left(0 \leq \xi \leq \frac{\zeta(t)}{b}\right) \qquad \text{(C1)}$$

where the magnitude of the velocity V_0 is a function of the projectile and plate parameters (see eq. (5)),

$$V_0 = \frac{\frac{2a}{h}\frac{\rho_p}{\rho_t}g_0}{1 + \frac{2a}{h}\frac{\rho_p}{\rho_t}\psi}$$

and $\zeta(t)$ is the radius of the hinge circle separating regimes A and AB, and $\xi = r/b$.

In the surrounding annulus of the remaining portion of the plastic plate (designated regime AB of the Tresca yield hexagon in fig. 9), the proper velocity distribution according to the dictates of rigid-plastic theory (see ref. 4) is linear in ξ, continuous

across the plate, and zero at the simply supported edge. The satisfaction of these conditions leads to the following expression for the velocity distribution in regime AB:

$$\dot{w}(\eta,0) = V_o\sqrt{1 - \left(\frac{b}{a}\right)^2\left(\frac{\zeta}{b}\right)^2}\,\frac{1 - \xi}{1 - \frac{\zeta}{b}} \qquad \left(\frac{\zeta}{b} \leqq \xi \leqq 1\right) \qquad \text{(C2)}$$

From the symmetry of the impulse loading it follows that the only nonvanishing stresses (on a circular plate element) are σ_r and σ_θ and the transverse shear-stress resultant Q_r. Summation of the vertical forces and summation of the moments acting on the plate result in the following equation of motion:

$$\frac{\partial}{\partial\xi}\left(\xi M_r\right) = M_\theta + b^2\int_0^\xi (\mu\ddot{w} - q)\,\xi\,d\xi \qquad \text{(C3)}$$

where the impulse loading q is prescribed by

$$q = \mu V_o\sqrt{1 - \left(\frac{b}{a}\right)^2\xi^2}\,\delta(t)$$

Equation (C3) is automatically satisfied by equation (C1) and reduces to $\mu\ddot{w} = q$ since $M_r = M_\theta = M_o$ in regime A of the Tresca yield hexagon (see ref. 4). In regime AB the equation of motion (eq. (C3)) is not uniquely satisfied until the radius of the hinge circle $\zeta(t)$ is determined. In order to solve for the proper time variation of $\zeta(t)$, the equation of motion is utilized with the velocity expression (eq. (C2)) and the associated boundary conditions for the surrounding annular region to obtain the following first-order total differential equation in $\zeta(t)/b$:

$$\frac{12M_o}{\mu V_o b^2}\,dt = \frac{1 - \left(\frac{b}{a}\right)^2\frac{\zeta}{b}}{\left[1 - \left(\frac{b}{a}\right)^2\left(\frac{\zeta}{b}\right)^2\right]^{1/2}}\left[-1 - 2\frac{\zeta}{b} + 3\left(\frac{\zeta}{b}\right)^2\right]d\left(\frac{\zeta}{b}\right) \qquad \text{(C4)}$$

where the associated boundary conditions of regime AB are

$$M_r\left(\frac{\zeta}{b},t\right) = M_o$$

$$M_r(1,t) = 0 \qquad \text{(C5)}$$

APPENDIX C

Integration of equation (C4) yields

$$\frac{12M_o}{\mu V_o b^2}t + C_1 = \left[1 - \left(\frac{b}{a}\right)^2\left(\frac{\zeta}{b}\right)^2\right]^{1/2}\left[-1 + 4\left(\frac{a}{b}\right)^2 - \frac{\zeta}{b} + \left(\frac{\zeta}{b}\right)^2 - \frac{3}{2}\left(\frac{a}{b}\right)^2\frac{\zeta}{b}\right] + \frac{3}{2}\left(\frac{a}{b}\right)^3 \sin^{-1}\frac{\zeta/b}{a/b} \quad \text{(C6)}$$

where C_1 is the constant of integration.

The initial location of the hinge-circle radius $\zeta(0)/b$ is determined from two requirements: (1) that the time rates of curvature $\dot{k}_r$ and $\dot{k}_\theta$ be nonnegative in regime A, and (2) that $d(\zeta/b)/dt$ (eq. (C4)) be negative. The first condition of nonnegative time rates of curvature is satisfied by the initial velocity distribution in regime A for $0 \leqq \xi \leqq a/b$. (See eq. (C1).) However, if the initial hinge circle radius is taken equal to a/b, then $d(\zeta/b)/dt$ would be zero, would indicate no movement of the radial position of $\zeta(t)/b$ with time, and no decrease in the total kinetic energy of the sheet and hence, no plastic deformation. If the position of $\zeta(0)/b$ is taken to lie between $(a/b)^2$ and a/b the rate of hinge-circle movement, $d(\zeta/b)/dt$, is positive and the radial position of $\zeta(t)/b$ increases with time until it reaches the position a/b where the hinge-circle movement ceases once again. If, however, the maximum value of $\zeta(0)/b$ which yields a negative value of $d(\zeta/b)/dt$ is determined, the kinetic energy of the plate will decrease as $\zeta(t)/b$ decreases and the time rates of curvature $\dot{k}_r$ and $\dot{k}_\theta$ will be nonnegative also. Hence, solving equation (C4) for the largest value of $\zeta(0)/b$ for which $d(\zeta/b)/dt$ is negative yields

$$\left(\frac{a}{b}\right)^2 - \frac{\zeta(0)}{b} = 0$$

or

$$\frac{\zeta(0)}{b} = \left(\frac{a}{b}\right)^2 \qquad \left(0 \leqq \frac{a}{b} \leqq 1\right) \quad \text{(C7)}$$

For values of $\frac{a}{b} > 1$, the hinge circle remains at the outer edge of the sheet since the simple support boundary condition $M_r(b,t) = 0$ (eq. (C5)) prohibits regime A from encompassing the edge of the plate and passing beyond. Hence for $\frac{a}{b} \geqq 1$,

$$\frac{\zeta(0)}{b} = 1 \quad \text{(C8)}$$

The value of $t = t_1$, at the time the hinge circle vanishes at the center of the sheet, can be determined from equation (C6) by first evaluating C_1 (by setting $t = 0$ and $\frac{\zeta}{b} = \frac{\zeta(0)}{b}$ (eqs. (C7) or (C8))) and then setting $\frac{\zeta}{b} = 0$ to yield

APPENDIX C

$$\frac{24M_o}{\mu V_o b^2} t_1 = -2 + 8\left(\frac{a}{b}\right)^2 + \sqrt{1 - \left(\frac{a}{b}\right)^2}\left[2 - 6\left(\frac{a}{b}\right)^2 + \left(\frac{a}{b}\right)^4\right] - 3\left(\frac{a}{b}\right)^3 \sin^{-1}\frac{a}{b} \qquad \left(0 \leqq \frac{a}{b} \leqq 1\right) \tag{C9}$$

and

$$\frac{24M_o}{\mu V_o b^2} t_1 = -2 + 8\left(\frac{a}{b}\right)^2 + \sqrt{1 - \left(\frac{b}{a}\right)^2}\left[2 - 5\left(\frac{a}{b}\right)^2\right] - 3\left(\frac{a}{b}\right)^3 \sin^{-1}\frac{b}{a} \qquad \left(\frac{a}{b} \geqq 1\right) \tag{C10}$$

In general, for $\frac{\zeta}{b} = \xi$, equation (C6) becomes

$$\frac{24M_o}{\mu V_o b^2} t(\xi) = \left[1 - \left(\frac{\xi}{a/b}\right)^2\right]^{1/2}\left[-2 + 8\left(\frac{a}{b}\right)^2 - 2\xi + 2\xi^2 - 3\left(\frac{a}{b}\right)^2\xi\right] + 3\left(\frac{a}{b}\right)^3 \sin^{-1}\left(\frac{\xi}{a/b}\right) + 2 - 8\left(\frac{a}{b}\right)^2 + \frac{24M_o}{\mu V_o b^2} t_1 \tag{C11}$$

The deflection of the plate with a hinge circle of finite radius can now be determined since the velocities of deformation have been established. The deflection of the surrounding annulus of the plastically deforming sheet, from $\frac{\zeta(0)}{b} \leqq \xi \leqq 1$, which has always remained in plastic regime AB (eq. (C2)) is

$$w(\xi,t_1) = \int_0^{t_1} V_o\left[1 - \left(\frac{b}{a}\right)^2\left(\frac{\zeta}{b}\right)^2\right]^{1/2} \frac{1 - \xi}{1 - \frac{\zeta}{b}}\, dt \qquad \left(\frac{\zeta(0)}{b} \leqq \xi \leqq 1\right) \tag{C12}$$

The central portion of the plastic sheet contains sheet elements that are first located in the plastic regime A and then, as the hinge-circle passes over them, in the plastic regime AB. The deflection is, therefore, dependent upon the time integration of two velocities: one velocity when the point in question is in regime A (eq. (C1)), and the second velocity (after time $t(\xi)$ when the hinge circle passes over that point $\left(\frac{\zeta}{b} = \xi\right)$) when the point is in regime AB (eq. (C2)). Hence,

$$w(\xi,t_1) = V_o\sqrt{1 - \left(\frac{b}{a}\right)^2\xi^2}\, t(\xi) + \int_{t(\xi)}^{t_1} V_o\sqrt{1 - \left(\frac{b}{a}\right)^2\left(\frac{\zeta}{b}\right)^2}\, \frac{1 - \xi}{1 - \frac{\zeta}{b}}\, dt \qquad \left(0 \leqq \xi \leqq \frac{\zeta(0)}{b}\right) \tag{C13}$$

Expressing dt in terms of $d(\zeta/b)$ (eq. (C4)) and integrating equations (C12) and (C13) yields

$$w(\xi,t_1) = \frac{\mu V_o^2 b^2}{24 M_o}(1 - \xi)\left[\left(\frac{a}{b}\right)^2 + \left(\frac{a}{b}\right)^4\right] \qquad \left(\frac{\zeta(0)}{b} \leqq \xi \leqq 1\right) \tag{C14}$$

$$w(\xi,t_1) = V_o\sqrt{1 - \left(\frac{b}{a}\right)^2 \xi^2}\, t(\xi) + \frac{\mu V_o^2 b^2}{24 M_o}(1 - \xi)\left[2\xi + 3\xi^2 - \left(\frac{b}{a}\right)^2 \xi^2 - 2\left(\frac{b}{a}\right)^2 \xi^3\right]$$

$$\left(0 \leqq \xi \leqq \frac{\zeta(0)}{b}\right) \tag{C15}$$

where $t(\xi)$ is given by equation (C11).

Solution With Hinge Circle of Zero Radius

When the hinge circle radius shrinks to zero at $t = t_1$ and the entire plate is in the plastic regime AB, the previous analysis must be terminated because the acceleration of the plate vanishes and the equation of motion (see eq. (C3)) reduces to

$$\frac{\partial}{\partial \xi}(\xi M_r) = M_o$$

or

$$M_r = M_o + \frac{C_3}{\xi} \tag{C16}$$

where C_3 is the constant of integration. Since $M_r = M_o$ at $\xi = 0$, $C_3 = 0$ and M_r remains at the constant yield-moment value of M_o in contradiction to the prescribed plasticity condition in regime AB (ref. 4) and the simply supported edge condition at $\xi = 1$ (eq. (C5)). It can be shown that the following expression for sheet deflection satisfies the plasticity and boundary conditions of the sheet, once the hinge-circle radius has shrunk to zero:

$$w(\xi,t) = \phi(t)\,(1 - \xi) + w(\xi,t_1) \qquad (t \geqq t_1) \tag{C17}$$

where $w(\xi,t_1)$ is the deflection at $t = t_1$, given by equations (C14) and (C15), and $\phi(t)$ is an arbitrary function of time.

Again, the acceleration is obtained by differentiation of equation (C17) and is substituted into equation (C3) with $M_\theta = M_o$. The subsequent integration of equation (C3) and application of the boundary conditions:

APPENDIX C

$$\left.\begin{aligned} M_r &= M_o \qquad (\xi = 0) \\ M_r &= 0 \qquad (\xi = 1) \end{aligned}\right\} \tag{C18}$$

yield

$$\ddot{\phi} = \frac{-12M_o}{\mu b^2} \tag{C19}$$

which, upon integration by utilizing the conditions evaluated at $t = t_1$,

$$\left.\begin{aligned} \phi(t_1) &= 0 \\ \dot{\phi}(t_1) &= V_o \end{aligned}\right\} \tag{C20}$$

becomes

$$\phi(t) = -\frac{6M_o}{\mu b^2}(t - t_1)^2 + V_o(t - t_1) \tag{C21}$$

Hence, the deflection for $t \geq t_1$ is

$$w(\xi,t) = w(\xi,t_1) + (1 - \xi)\left[\frac{-6M_o}{\mu b^2}(t - t_1)^2 + V_o(t - t_1)\right] \qquad (t \geq t_1) \tag{C22}$$

The time $t = t^*$ at which the entire plate comes to rest can be found by differentiating equation (C22) to obtain the velocity, by equating the resulting expression for velocity to zero, and then solving for t^*. This procedure yields

$$\frac{12M_o}{\mu V_o b^2} t^* = 1 + \frac{12M_o}{\mu V_o b^2} t_1 \tag{C23}$$

and the permanent deformation shape, denoted as $w^*(\xi,t^*)$ for $t \geq t^*$, can then be written as

$$w^*(\xi,t^*) = w(\xi,t_1) + (1 - \xi)\frac{\mu V_o^2 b^2}{24M_o} \tag{C24}$$

The permanent center deformation becomes (eqs. (C15) and (C24) with $\xi = 0$)

$$w^*(0,t^*) = \delta = \frac{\mu V_o^2 b^2}{24M_o}\left(1 + \frac{24M_o}{\mu V_o b^2} t_1\right) \tag{C25}$$

REFERENCES

1. Souter, Robert K.; and Emerson, Joseph B.: Summary of Available Hail Literature and the Effect of Hail on Aircraft in Flight. NACA TN 2734, 1952.

2. Anon.: Tentative Airworthiness Standards for Supersonic Transports. Flight Standards Service, FAA, Nov. 1, 1965; Revision 4, Dec. 29, 1967.

3. Hayduk, Robert J.: The Response of a Single Wall Space Structure to Impact by Cometary Meteoroids of Various Shapes. M.S. Thesis, Virginia Polytech. Inst., 1968.

4. Thomson, Robert G.: Plastic Behavior of Circular Plates Under Transverse Impulse Loadings of Gaussian Distribution. NASA TR R-279, 1968.

5. Comm. on Metric Pract.: ASTM Metric Practice Guide. NBS Handbook 102, U.S. Dep. Com., Mar. 10, 1967.

6. Medick, M. A.: On Classical Plate Theory and Wave Propagation. ASME, Ser. E: J. Appl. Mech., vol. 28, no. 2, June 1961, pp. 223-228.

7. Hayduk, Robert J.: Response of an Infinite Elastic Plate to Axisymmetric Initial Velocity Distributions With Application to Hypervelocity Impact. NASA TN D-5118, 1969.

8. Thomson, Robert G.; and Kruszewski, E. T.: Effect of Target Material Yield Strength on Hypervelocity Perforation and Ballistic Limit. Proceedings of the Seventh Hypervelocity Impact Symposium, vol. V, Feb. 1965, pp. 273-320. (Sponsored by U.S. Army, U.S. Air Force, and U.S. Navy.)

9. Fish, Richard H.; and Summers, James L.: The Effect of Material Properties on Threshold Penetration. Proceedings of the Seventh Hypervelocity Impact Symposium, vol. VI, Feb. 1965, pp. 1-26. (Sponsored by U.S. Army, U.S. Air Force, and U.S. Navy.)

10. Alfaro-Bou, Emilio; and Thomson, Robert G.: Ballistic Limit of Aluminum Plates Determined by an Exploding Foil Gun Technique. NASA TN D-4259, 1967.

TABLE I.- TARGET AND PROJECTILE MATERIAL PROPERTIES AND VALUES OF THE MOMENTUM CONSTANT ψ

(a) Target and projectile material properties

Property	U.S. unit	SI unit
Target material (2024-T4 aluminum)		
Yield stress, σ_o	68 000 psi	0.47 GN/m^2
Modulus of elasticity, E . . .	10.6×10^6 psi	73.1 GN/m^2
Density, ρ_t	5.37 $slugs/ft^3$	2767 kg/m^3
$c = \sqrt{E/\rho_t}$	16 900 ft/sec	5.15 km/s
Projectile		
Density, ρ_p	1.78 $slugs/ft^3$	917 kg/m^3
Specific gravity	0.916	0.916

(b) Values of the momentum constant ψ computed from equation (7)

Target thickness, h		Values of ψ at various projectile radii		
in.	cm	a = 0.50 in. (1.27 cm)	a = 0.25 in. (0.64 cm)	a = 0.125 in. (0.32 cm)
0.063	0.160	0.70	0.71	0.72
.04	.10	.69	.70	.71

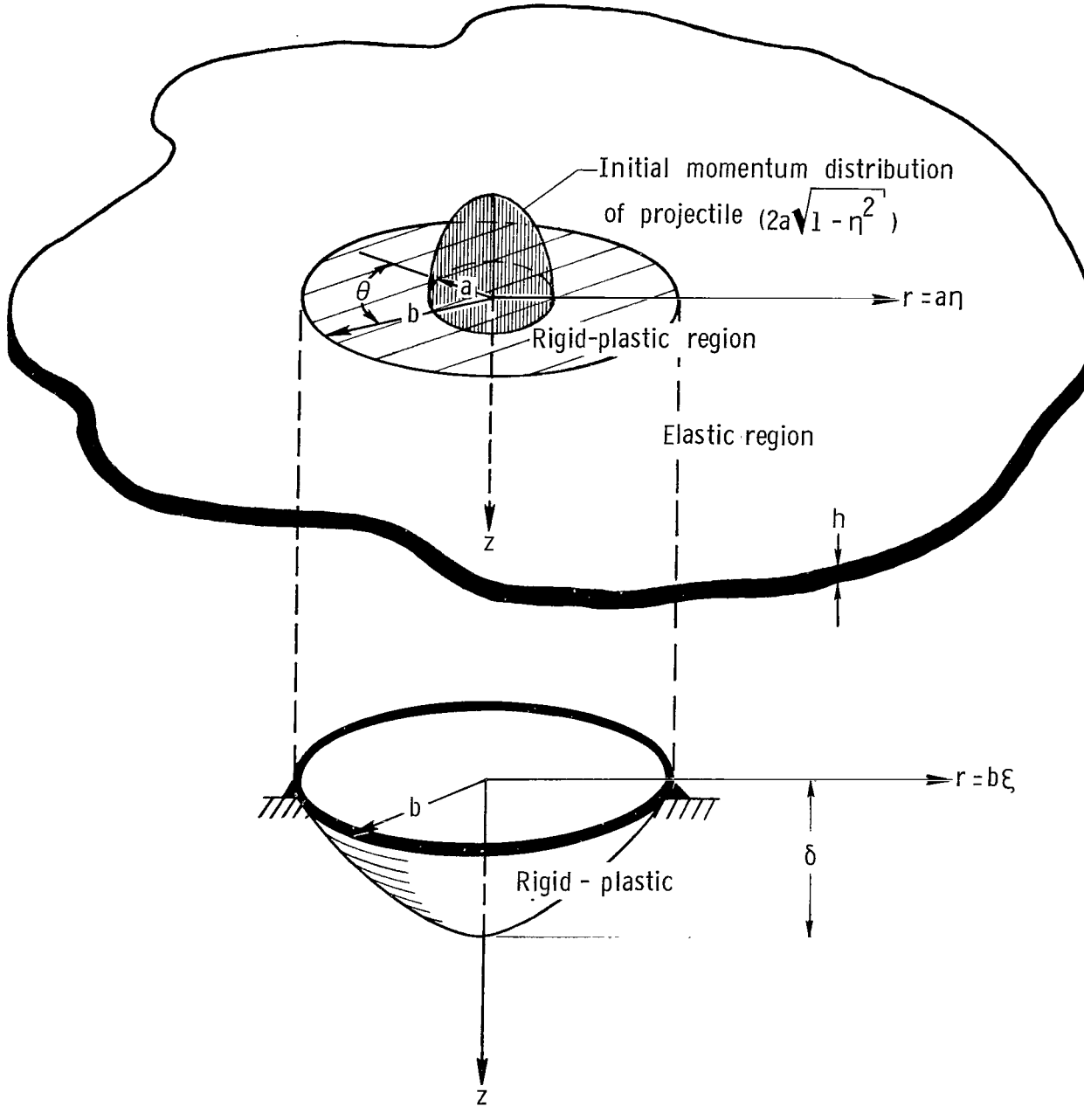

Figure 1.- Elastic and rigid-plastic regions.

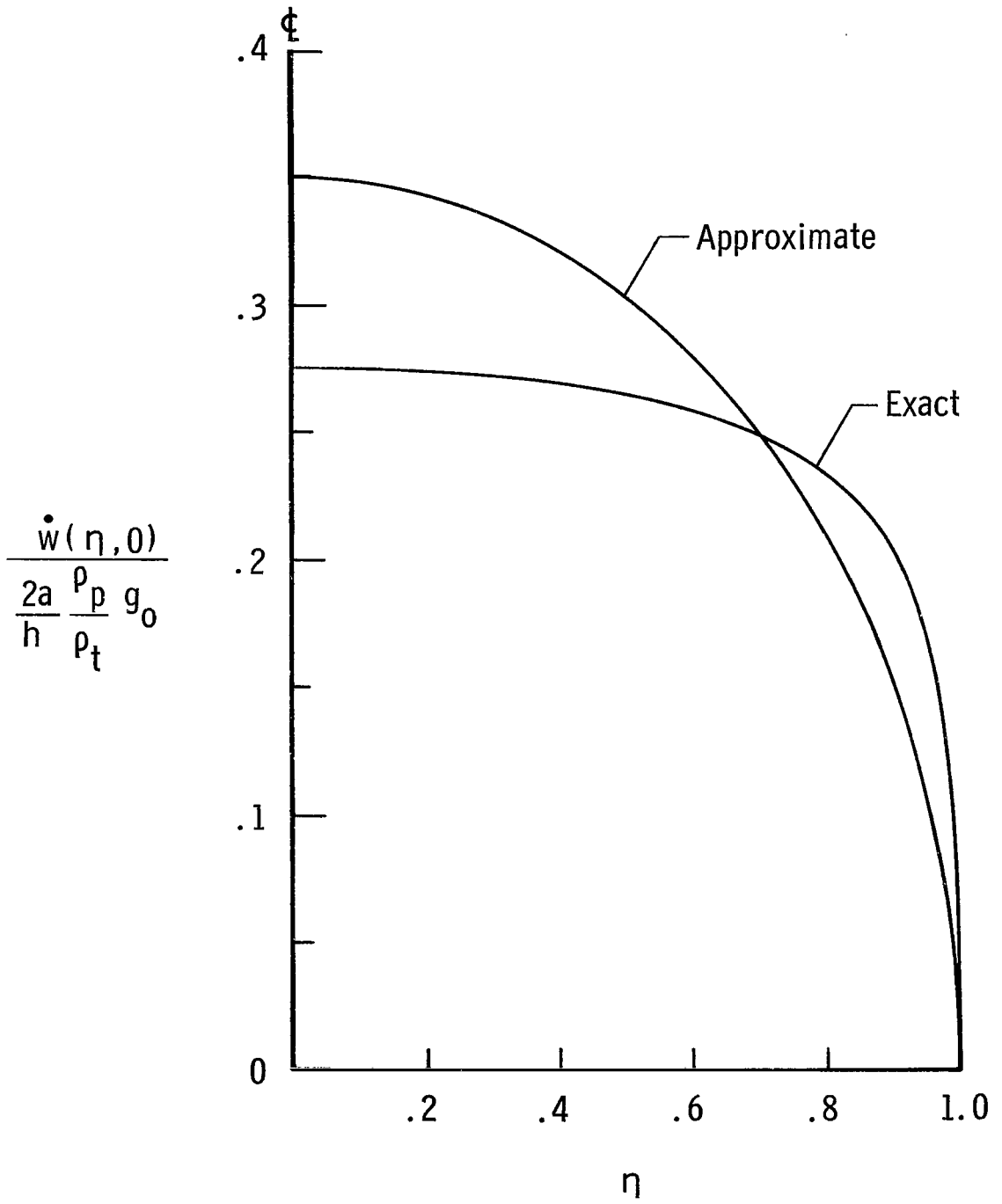

Figure 2.- Initial velocity distribution resulting from momentum balance between the spherical projectile and the target plate.

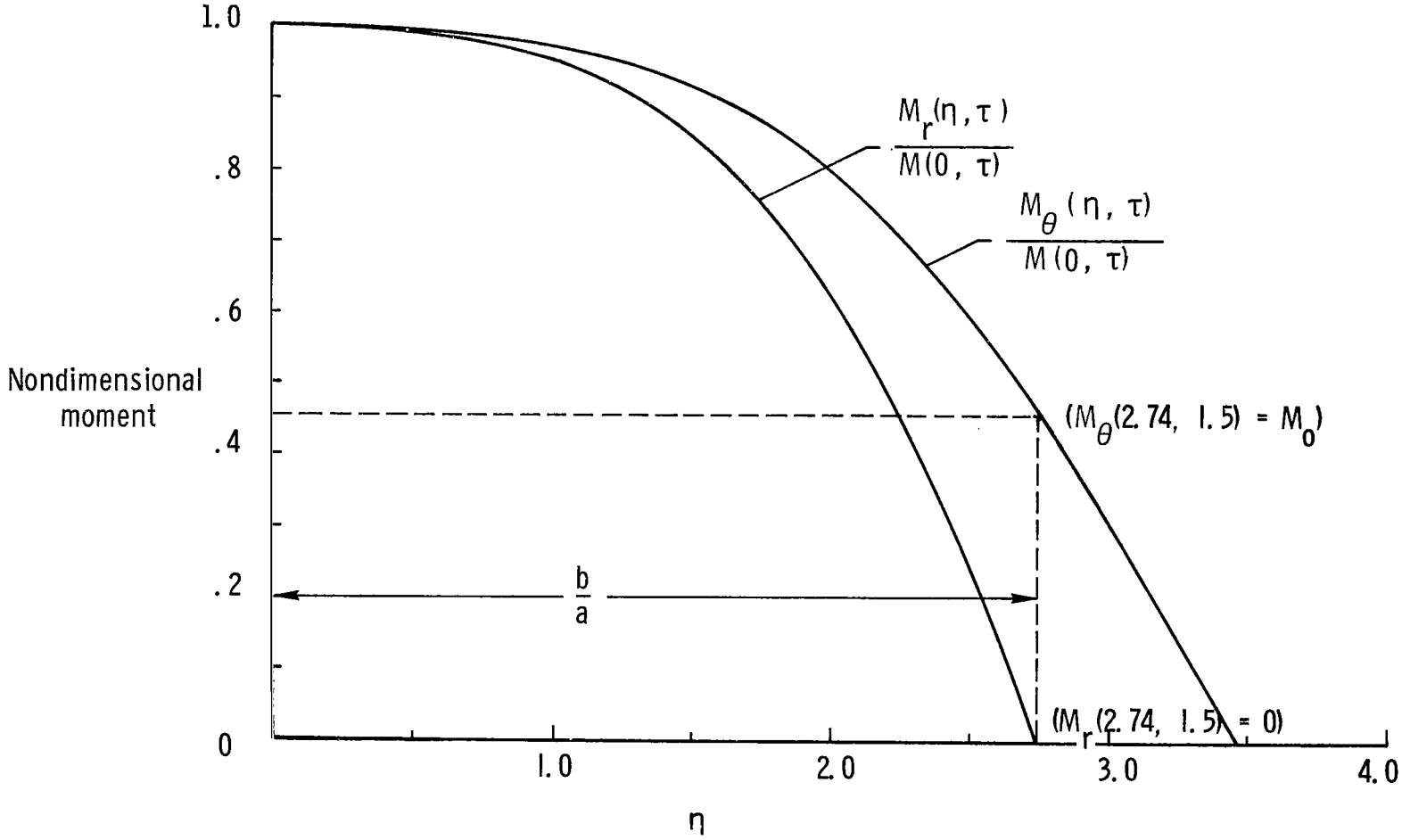

Figure 3.- Typical moment distributions in central portion of infinite elastic plate. $\tau = 1.5$.

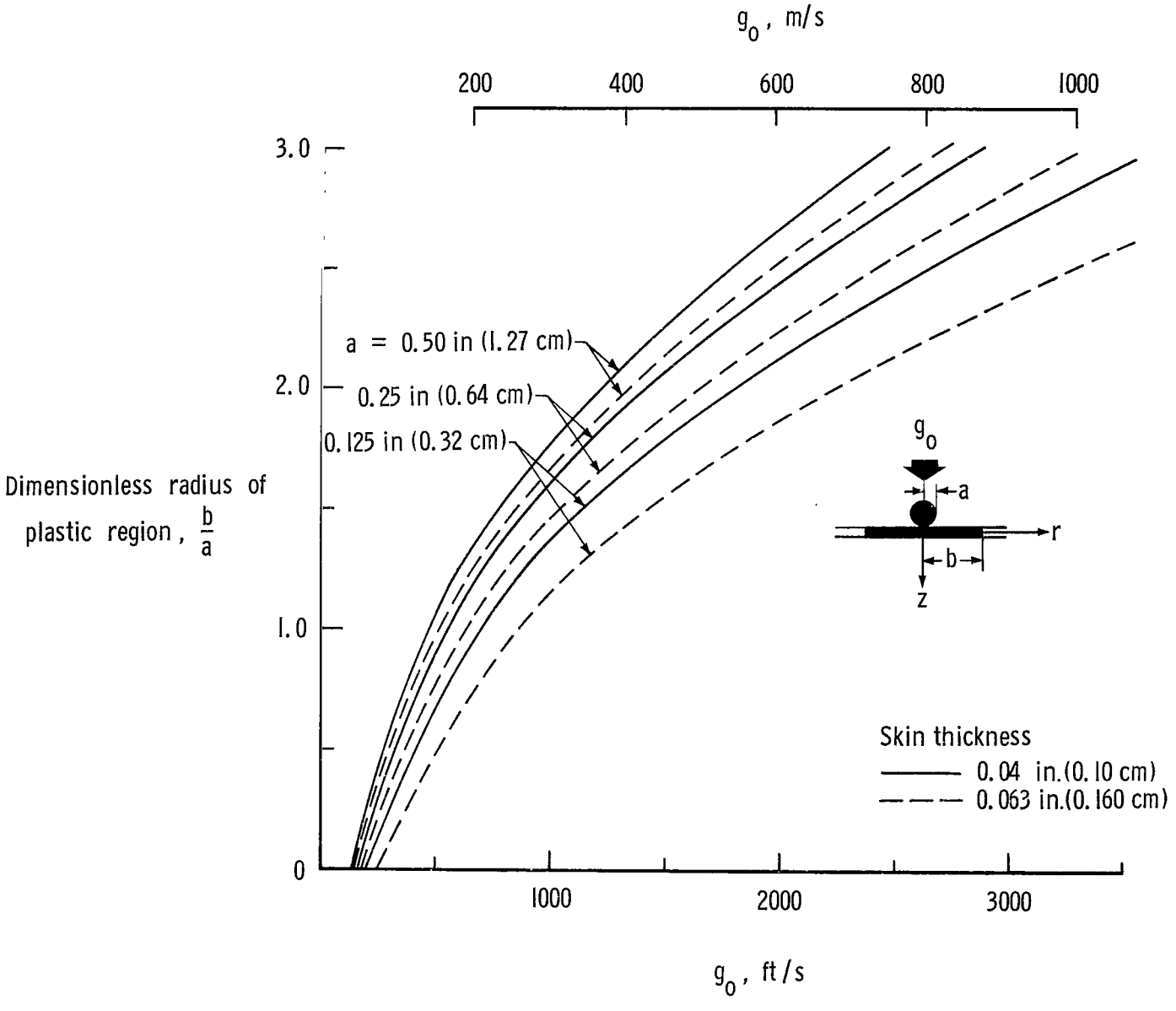

Figure 4.- Radius of plastic region as a function of projectile velocity.

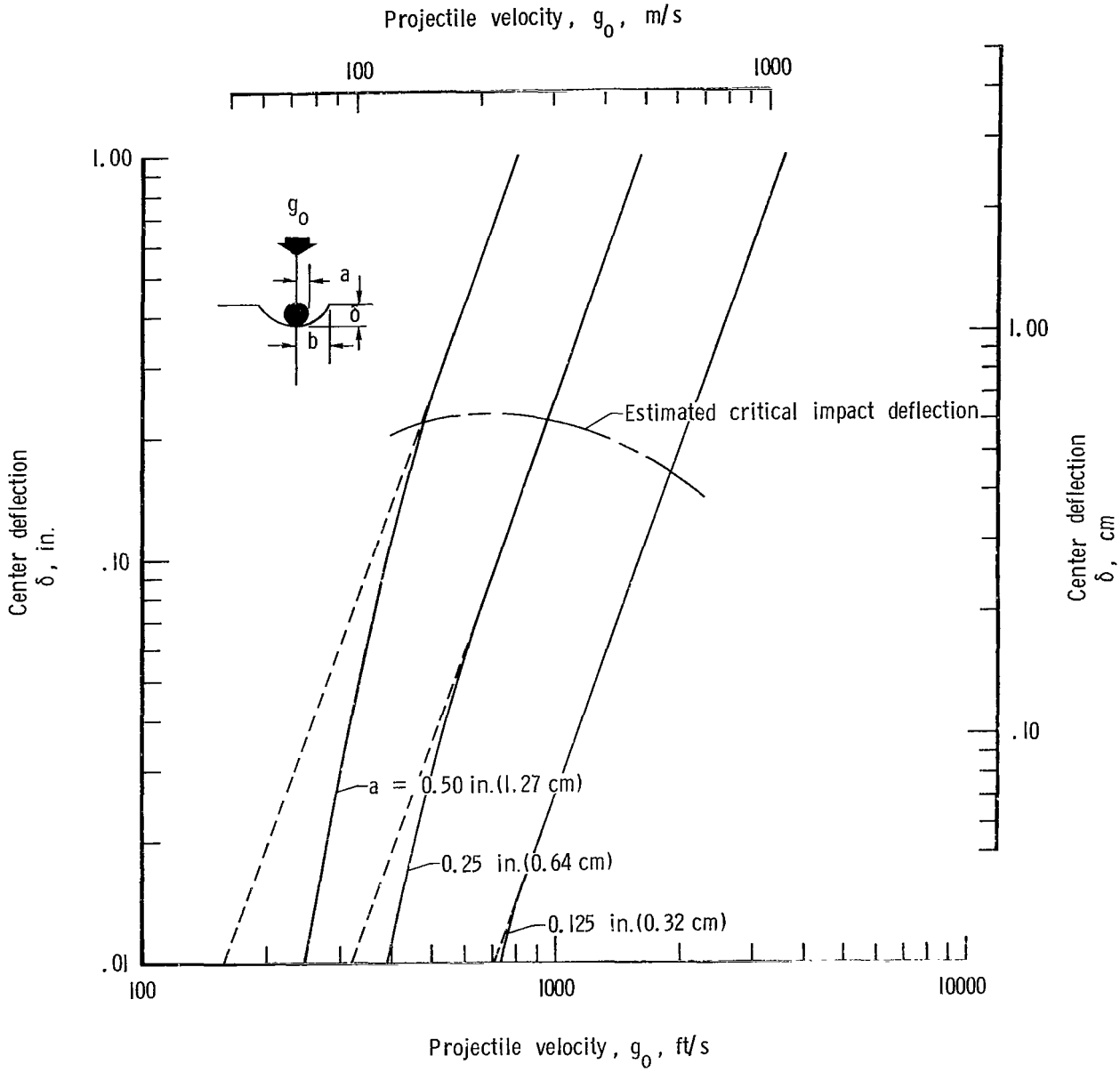

Figure 5.- Center deflection δ as a function of projectile velocity g_0. 0.063-inch-thick (0.160-cm) 2024-T4 aluminum sheet; $\delta \propto g_0^{2.85}$.

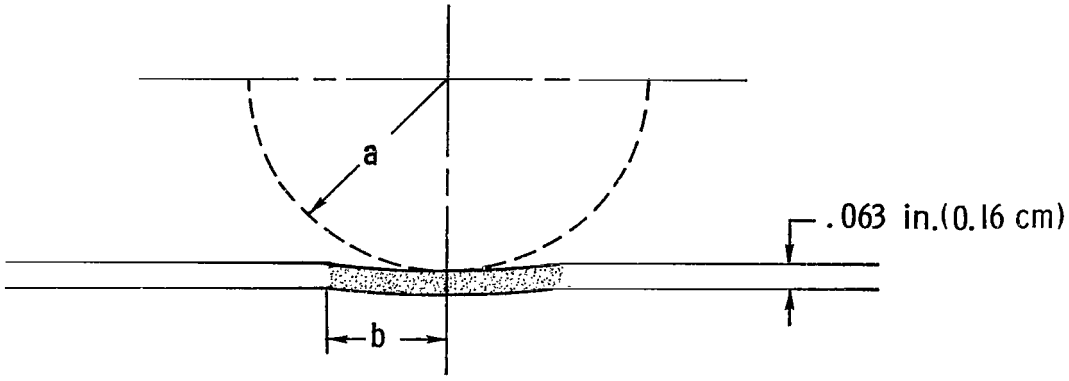

(a) Impact velocity, 330 ft/sec (0.10 km/s).

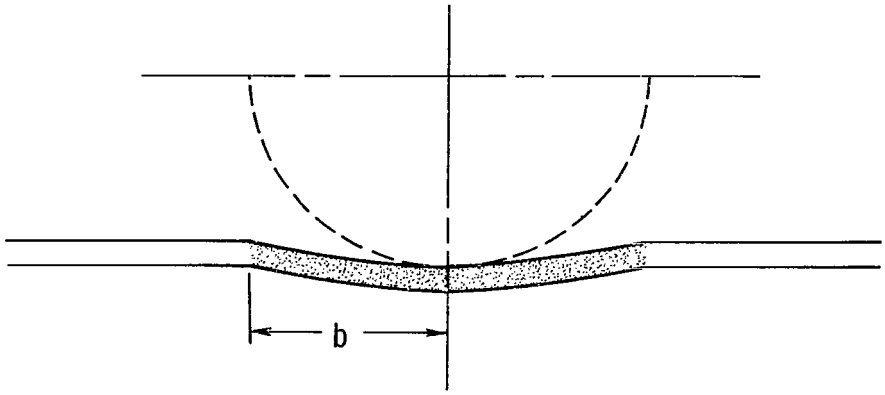

(b) Impact velocity, 500 ft/sec (0.15 km/s).

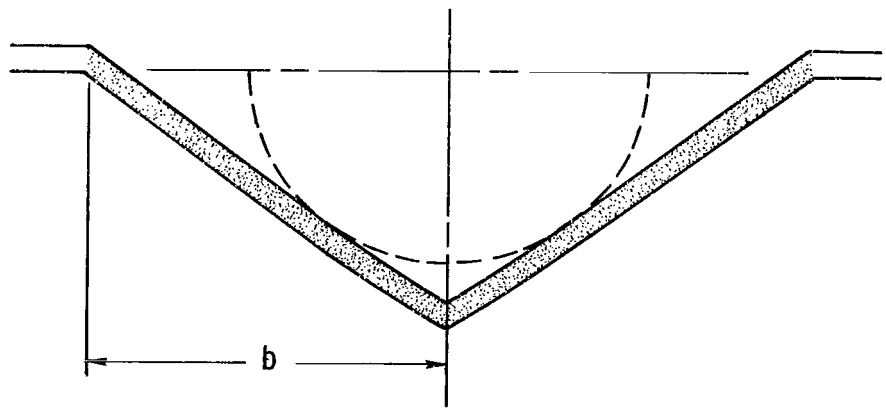

(c) Impact velocity, 1100 ft/sec (0.34 km/s).

Figure 6.- Variation in permanent deflection of 2024-T4 aluminum sheet impacted with 1-inch-diameter projectile at various velocities. a = 0.50 in. (1.27 cm).

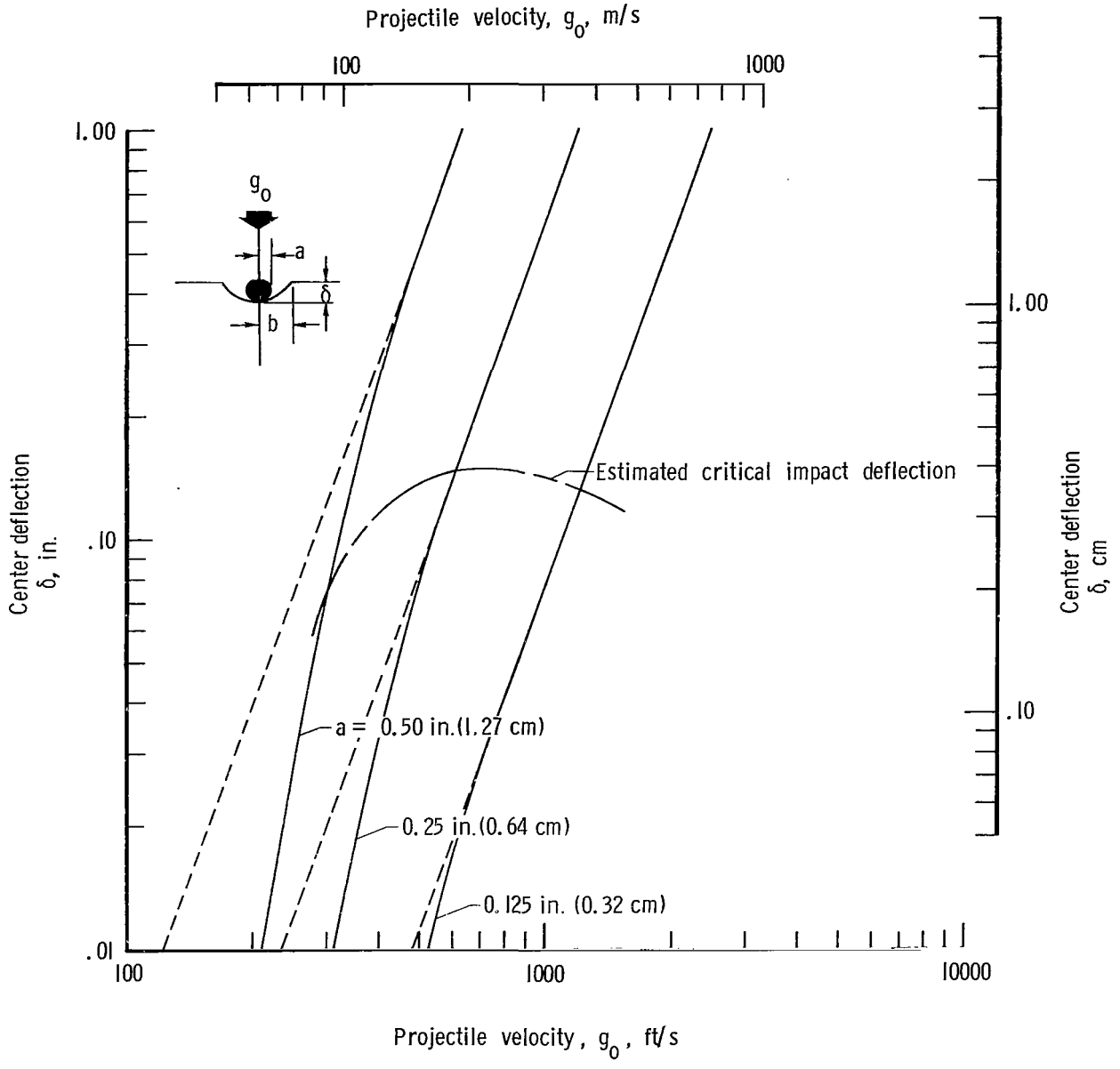

Figure 7.- Center deflection δ as a function of projectile velocity g_0. 0.04-inch-thick (0.10-cm) 2024-T4 aluminum sheet; $\delta \propto g_0^{2.85}$.

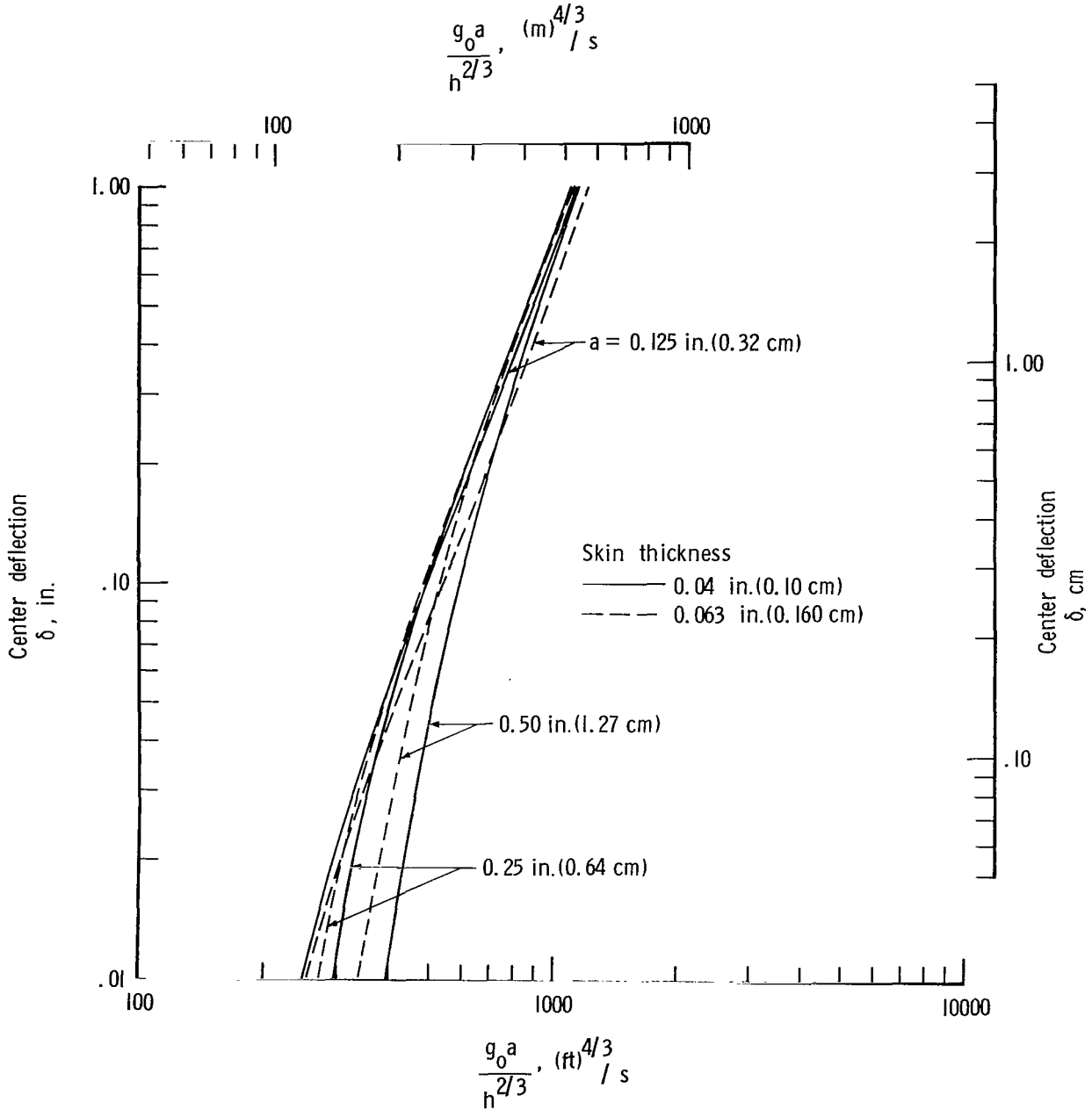

Figure 8.- Center deflection δ as a function of $\frac{g_0 a}{h^{2/3}}$.

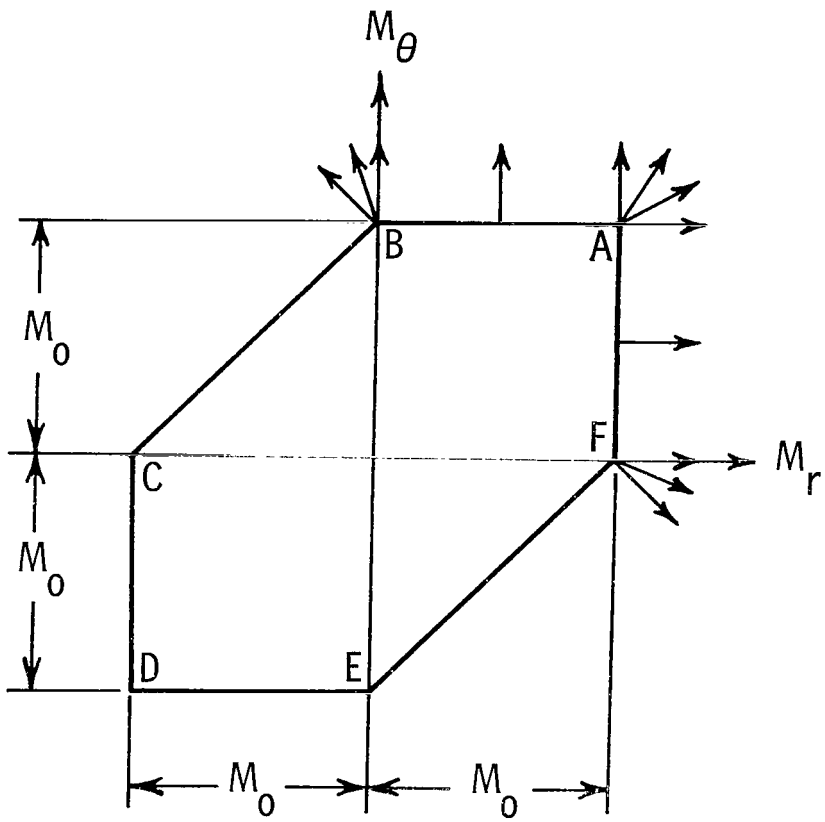

Figure 9.- Tresca yield hexagon.

NASA-Langley, 1969 —— 32 L-6494

NATIONAL AERONAUTICS AND SPACE ADMINISTRATION
WASHINGTON, D.C. 20546

OFFICIAL BUSINESS

FIRST CLASS MAIL

POSTAGE AND FEES PAID
NATIONAL AERONAUTICS AND
SPACE ADMINISTRATION

"The aeronautical and space activities of the United States shall be conducted so as to contribute . . . to the expansion of human knowledge of phenomena in the atmosphere and space. The Administration shall provide for the widest practicable and appropriate dissemination of information concerning its activities and the results thereof."

—NATIONAL AERONAUTICS AND SPACE ACT OF 1958

NASA SCIENTIFIC AND TECHNICAL PUBLICATIONS

TECHNICAL REPORTS: Scientific and technical information considered important, complete, and a lasting contribution to existing knowledge.

TECHNICAL NOTES: Information less broad in scope but nevertheless of importance as a contribution to existing knowledge.

TECHNICAL MEMORANDUMS: Information receiving limited distribution because of preliminary data, security classification, or other reasons.

CONTRACTOR REPORTS: Scientific and technical information generated under a NASA contract or grant and considered an important contribution to existing knowledge.

TECHNICAL TRANSLATIONS: Information published in a foreign language considered to merit NASA distribution in English.

SPECIAL PUBLICATIONS: Information derived from or of value to NASA activities. Publications include conference proceedings, monographs, data compilations, handbooks, sourcebooks, and special bibliographies.

TECHNOLOGY UTILIZATION PUBLICATIONS: Information on technology used by NASA that may be of particular interest in commercial and other non-aerospace applications. Publications include Tech Briefs, Technology Utilization Reports and Notes, and Technology Surveys.

Details on the availability of these publications may be obtained from:

SCIENTIFIC AND TECHNICAL INFORMATION DIVISION

NATIONAL AERONAUTICS AND SPACE ADMINISTRATION

Washington, D.C. 20546